Physica Medica 124 (2024) 103421

Contents lists available at ScienceDirect

Physica Medica

journal homepage: www.elsevier.com/locate/ejmp

Original paper

A dosiomics approach to treatment outcome modeling in carbon ion radiotherapy for skull base chordomas

Giovanni Parrella [a,*], Simone Annunziata [a], Letizia Morelli [a], Silvia Molinelli [b], Giuseppe Magro [b], Mario Ciocca [b], Giulia Riva [c], Lucia Pia Ciccone [c], Alberto Iannalfi [c], Chiara Paganelli [a], Ester Orlandi [d,e], Guido Baroni [a]

[a] Politecnico di Milano, Department of Electronics, Information and Bioengineering, Milano, Italy
[b] Centro Nazionale di Adroterapia Oncologica, Medical Physics Unit, Pavia, Italy
[c] Centro Nazionale di Adroterapia Oncologica, Radiotherapy Unit, Pavia, Italy
[d] Centro Nazionale di Adroterapia Oncologica, Radiation Oncology Clinical Unit, Pavia, Italy
[e] University of Pavia, Department of Clinical, Surgical, Diagnostic and Pediatric Sciences, Pavia, Italy

ARTICLE INFO

Keywords:
Dosiomics
Tumor control probability
Skull-base chordomas
Carbon ion radiotherapy

ABSTRACT

Purpose: To investigate the role of dosiomics features extracted from physical dose (D_{PHYS}), RBE-weighted dose (D_{RBE}) and dose-averaged Linear Energy Transfer (LET_d), to predict the risk of local recurrence (LR) in skull base chordoma (SBC) treated with Carbon Ion Radiotherapy (CIRT). Thus, define and evaluate dosiomics-driven tumor control probability (TCP) models.

Materials and methods: 54 SBC patients were retrospectively selected for this study. A regularized Cox proportional hazard model (r-Cox) and Survival Support Vector Machine (s-SVM) were tuned within a repeated Cross Validation (CV) and patients were stratified in low/high risk of LR. Models' performance was evaluated through Harrell's concordance statistic (C-index), and survival was represented through Kaplan-Meier (KM) curves. A multivariable logistic regression was fit to the selected feature sets to generate a dosiomics-driven TCP model for each map. These were compared to a reference model built with clinical parameters in terms of f-score and accuracy.

Results: The LETd maps reached a test C-index of 0.750 and 0.786 with r-Cox and s-SVM, and significantly separated KM curves. D_{PHYS} maps and clinical parameters showed promising CV outcomes with C-index above 0.8, despite a poorer performance on the test set and patients stratification. The LETd-based TCP showed a significatively higher f-score (0.67[0.52–0.70], median[IQR]) compared to the clinical model (0.4[0.32–0.63], $p < 0.025$), while D_{PHYS} achieved a significatively higher accuracy (D_{PHYS}: 0.73[0.65–0.79], Clinical: 0.6 [0.52–0.72]).

Conclusion: This analysis supports the role of LETd as relevant source of prognostic factors for LR in SBC treated with CIRT. This is reflected in the TCP modeling, where LETd and D_{PHYS} showed an improved performance with respect to clinical models.

1. Introduction

Carbon ion radiotherapy (CIRT) is a well-established approach to treat radioresistant and deep-seated tumors, such as skull base chordomas (SBC) [1–3]. Indeed, beyond the great geometrical selectivity in the dose deposition, the high linear energy transfer (LET) of carbon ions leads to a superior relative biological effectiveness (RBE), if compared to conventional radiotherapy.

Nonetheless, in the case of SBC the use of stringent dose constraints imposed on nearby organs at risk (OARs) may hinder the achievement of a uniform dose distribution on the target, resulting in areas of underdosage and high recurrence rates [2]. This, in combination with a poor characterization of SBC [4–6] and the lack of prognostic signatures, hampers the effectiveness and personalization of the treatments as well as an optimal patients' stratification.

In support to this, imaging biomarkers have been proved to be non-

* Corresponding author.
E-mail address: giovanni.parrella@polimi.it (G. Parrella).

https://doi.org/10.1016/j.ejmp.2024.103421
Received 26 November 2023; Received in revised form 23 April 2024; Accepted 29 June 2024
Available online 4 July 2024

invasive and clinically relevant prognostic factors [7], with the radiomics paradigm gaining importance as a tool to extract large amounts of quantitative features from medical images, and combine them with statistical or machine learning approaches to support outcome prediction and clinical decision making [8]. Similarly, an increasing interest is observed in the field dosiomics, where the radiomic approach is extended to encompass physical and biological parameters associated with the radiotherapy plan, such as dose maps (e.g., physical and RBE-weighted) and dose-weighted linear energy transfer (LETd) maps [9].

Few radiomics studies have been targeting SBC to date [10–12]. To our best knowledge, the work from Buizza et al. is the only one exploring both radiomic and dosiomic approaches to predict local control in SBC patients treated with CIRT [13]. The study highlights the potential role of dosiomics applied to RBE-weighted dose maps (D_{RBE}) in predicting treatment outcome, but no investigations were reported on physical dose (D_{PHYS}) and LET_d maps. In this regard, LET_d has been recently investigated as a relevant physical parameter for treatment optimization and evaluation [14,15], with LET_d distributions being related to adverse treatment outcome in chondrosarcomas and sacral chordomas for CIRT [14–16], thus also supporting LET-guided optimization [17–21].

In this context, the use of quantitative imaging and dose features can be employed in the development of data-driven predictive models such as Tumor Control Probability (TCP), aiming at providing a phenomenological description of local control, towards treatment personalization [22,23]. Indeed, this would allow overcoming the currently adopted mechanistic radiobiological models typically derived from in to vitro irradiation studies, which do not describe the in-vivo tumour pathophysiology. The integration of dosiomics signatures within data-driven TCPs has not been investigated in the literature for CIRT applications. In this regard, some attempts have been made to personalize TCP models both by integrating conventional analytical TCP models with biological (e.g. hypoxia, cellularity) and clinical (e.g. sex, age) variables [23–26], as well as by defining radiomics-based nomograms, which try to correlate the values from a radiomic score (i.e. linear combination of relevant radiomic features) with tumor control probabilities [27].

The proposed study aims at exploring the use of dosiomics applied to LETd and dose maps as a potential source of prognostic factors for predicting local recurrence (LR) in patients with SBC undergoing CIRT. Thus, the use of dosiomics features for the development of dosiomics-driven TCP models is investigated and compared to a reference model fitted on clinical parameters.

2. Materials and Methods

2.1. Data collection and elaboration

This retrospective study included fifty four patients affected by non-metastatic SBC treated with CIRT at the National Centre for Oncological Hadrontherapy (CNAO) between 2013 and 2017, after incomplete macroscopical surgical resection (n = 53) or biopsy only (n = 1). None of these received adjuvant conventional RT or previous treatments other than surgery. Inclusion criteria were: (i) a prescription dose of 70.4 Gy (RBE) delivered in 16 fractions, with a sequential boost scheme with target shrinkage after 9 fractions; (ii) any surgical resection degree; (iii) at least 12-months follow-up; (iv) the availability of complete dosimetric and clinical data. Exclusion criteria are summarized in supplementary material S0 while demographic data are collected in Table 1. The study was approved by the local ethical committee.

Treatment plans were optimized with the Syngo RT planning (Siemens AG Healthcare, Erlangen, Germany) treatment planning system (TPS), using a pencil beam algorithm and the local effect model (LEM-I) for RBE evaluation, with $\alpha/\beta = 2$ Gy. The dose was prescribed to the Low-Dose Clinical Target Volume (CTV_{LD}) for the first 9 fractions, and on the High-Dose CTV (CTV_{HD}) for the following 7. Dose distributions were recalculated on Raystation version 10B (Raysearch Laboratories, Stockholm, Sweden), and LET_d maps were calculated in water normalized to unit density, including primary particles, secondary fragments ($Z < 6$) and target recoils up to oxygen ($Z = 8$). Dose contributions from the 9 and 7 fractions were summed to obtain the overall biological and physical doses, while LETd maps were combined through a weighted sum, following the approach suggested by Matsumoto et al. [16].

Table 1
Clinical and demographic parameters.

	Relapsed	Control
Number of patients	18	36
Sex	11 / 7 (Male/Female)	25 / 11 (Male/Female)
	Median (range)	*Median (range)*
Age	68 (41–79)	56 (17–81)
Number of fields	2(13) – 3(3) – 4(2)	2(31) – 3(5)
	Median (range)	*Median (range)*
Follow-up time [months]	66 (30–96)	67 (31–113)
Time-to-recurrence [months]	39 (15–83)	–
GTV Volume (cc)	12.23 (0.86–33.05)	12.48 (0.4–87.4)
Brainstem involvement	6	8
Optic Pathways involvement	2	3

The gross tumor volume (GTV) and CTV_{HD} contours were manually delineated from expert radiation oncologists on treatment planning CT, with CTV_{HD} being defined adding a 3–5 mm safety margin to the GTV, according to both the anatomy and the surgical pathway. This high risk volume (i.e. CTV_{HD}) was considered as the volume of interest of the present work, being the target receiving the complete treatment (9 + 7 fractions) [2].

The treatment outcome was monitored at each follow-up and classified as local control (LC) or local recurrence (LR), with the former describing a local progression-free survival (favorable event) and the latter referred to a relapse or progression in the target volume (adverse event).

After a median time-to-recurrence of 39.07 months, LR was identified in 18 patients (33 %), while 36 patients (77 %) were included in the LC group (median follow-up time = 67.63 months).

2.2. Feature extraction and selection

A total of 107 dosiomics features (14 shape, 18 first-order and 75 texture, more details in Supplementary material S1) were extracted from D_{PHYS}, D_{RBE} and LET_d maps using PyRadiomics (v3.0.1), with no preprocessing (i.e. normalization, filtering). Texture features were obtained from gray level dependence matrix (GLDM, $n = 14$), gray level run length matrix (GLRLM, $n = 16$), gray level size zone matrix (GLSZM, $n = 16$), gray level co-occurrence matrix (GLCM, $n = 24$) and neighboring gray tone difference matrix (NGTDM, $n = 5$).

Feature extraction was performed with a fixed bin count of 128 bins for all the maps, in accordance with the Image Biomarker Standardization Initiative (IBSI, [28]).

A two steps feature selection was applied to avoid data redundance and overfitting: (i) features with a spearman correlation coefficient greater than 0.90 were discarded thus keeping the largest uncorrelated sets of features, then (ii) a least absolute shrinkage and selection operator (LASSO) was applied within a repeated 5-fold cross-validation (CV) routine, to select the 5 most relevant features for each map. The LASSO was implemented using python Sklearn module, with a regularisation parameter of 0.01 on the L1 norm.

In addition, clinical parameters including sex, GTV volume, brainstem and optic pathways involvement were collected for all patients. Fig. 1 reports the workflow of the study.

2.3. Time-to-event analysis

The prognostic power of dosiomics features and clinical parameters was investigated and compared considering survival models based on (i)

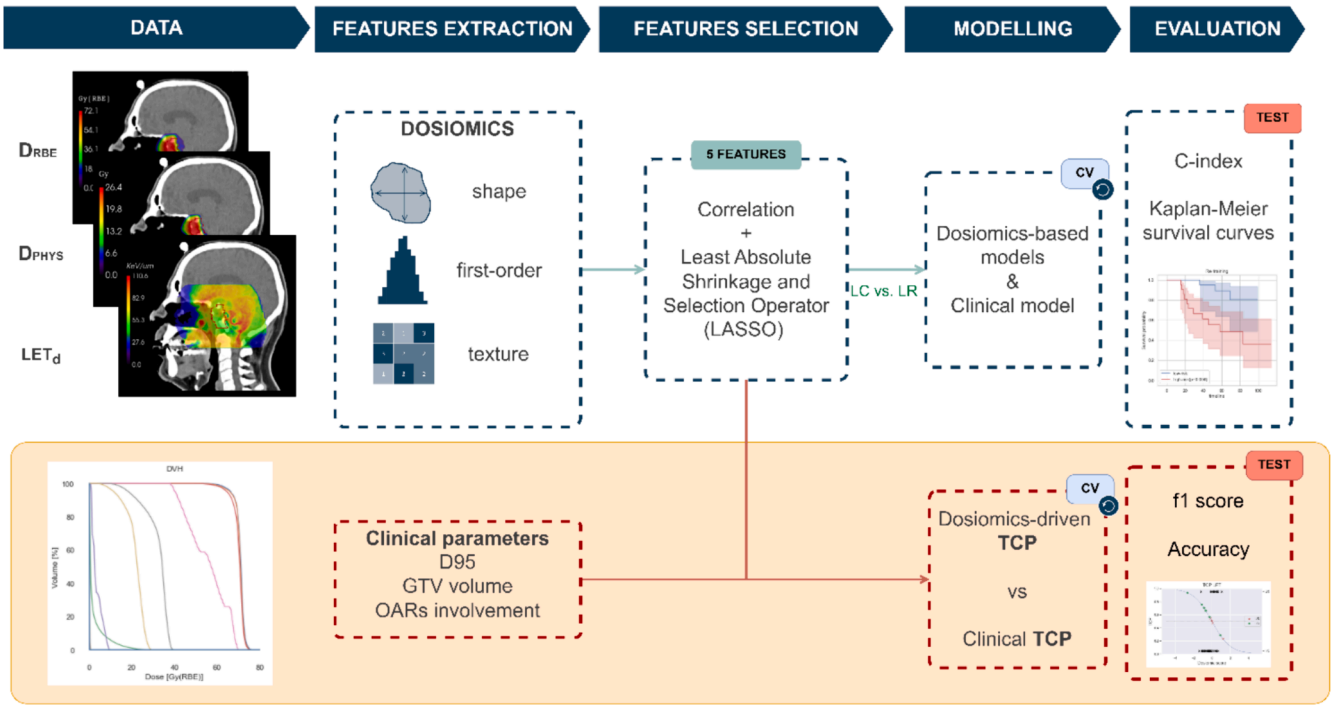

Fig. 1. Schematic representation of the workflow. Dosiomics features were extracted from D_{RBE}, D_{PHYS} and LET_d maps. A correlation filter and Least Absolute Shrinkage and Selection Operator (LASSO) were used as selection routines for dosiomics features. Time-to-event models based on r-Cox and s-SVM were tuned within a repeated 5-folds CV for LR prediction and evaluated in terms of C-index and KM curves on the test set. Dosiomics features and clinical parameters were fitted to a logit function (average model over a repeated 3-folds CV) to define data-driven TCP which were compared in terms of f1 score and accuracy on the test set.

linear survival support vector machine (s-SVM, scikit-survival v.0.18) and (ii) Cox proportional hazard model regularized with an elastic net penalty (r-Cox, scikit-survival v.0.18).

The dataset (n = 54) was split in train (80 %, n = 43) and test (20 %, n = 11). Dosiomics features were normalized using z-score and L2-norm for s-SVM and r-Cox, respectively. Hyper-parameters were tuned through a 10-times repeated 5-fold CV grid-search, by maximizing the Harrell's Concordance statistics (C-index) [29]. s-SVM and r-COX models were then fitted separately to the set of 5 selected dosiomics features, for each map.

The stratification of each patient of the test set into low/high risk of showing LR was obtained by setting the stratification cut-off to the median value of the model's output on the training set. This stratification allowed estimating Kaplan–Meier (KM) survival curves to predict recurrence-free survival.

The performance of the models was quantified through the C-index on the test-set as well as the median and interquartile range on cross-validation. The non-parametric Mann–Whitney *U* test ($\alpha = 0.05$) [30] was applied to investigate statistically significant differences among the performance of different maps in CV. The KM curves were compared using log-rank tests to test the model's ability to significantly separate patient groups, setting the significance at $\alpha = 0.05$. To account for multiple testing, a Bonferroni correction (n = 4) was applied to each model, thus leading to a corrected $\alpha = 0.0125$. The Mann–Whitney *U* test was applied to analyse statistically significant features among the LC/LR classes (i.e. ahead of stratification), as well as low- and high-risk groups employed for KM curves (i.e. downstream of stratification). This analysis allowed investigating the performance of dosiomics features and clinical parameters that were then employed in the definition of TCP models.

2.4. TCP models formulation

To simulate a clinical application, data-driven TCP models were formulated as a binary-classification problem between LC and LR classes, as reported by [23]. Specifically, a multivariable logistic regressor was tuned on the specific set of 5 optimal features selected for each map (i.e., D_{PHYS}, D_{RBE}, LET_d). Each dosiomics-based TCP model was optimized through a leave-one-out cross-validated grid-search and an average model was built within a 3-fold cross validation, repeated 5 times. Class imbalance was compensated through class weighting.

A clinical data-driven TCP model was similarly built considering the same parameters as in the time-to-event modeling, such as the GTV volume, sex, the brainstem and optic pathways involvement and the minimum dose received by the hottest 95 % of the volume (D95), which are suggested to be relevant prognostic factors for SBC [2].

$$TCP = \frac{100}{1 + e^{g(\boldsymbol{x})}} \tag{1}$$

$$g(\boldsymbol{x}) = \beta_0 + \sum_{i=1}^{N} \beta_i x_i \tag{2}$$

The TCP was defined as a logit function (Eq. (1)), with the dosiomics score ($g(\boldsymbol{x})$, Eq. (2) being defined as a linear combination of the features (i.e. the vector $\boldsymbol{x}$).

Each TCP, built on the training dataset (n = 43), was then evaluated by setting a TCP threshold of 50 % to discern among low- and high-risk cases on the test set (n = 11). The performance of such models was compared to the clinical one in terms of f-score and accuracy. Mann–Whitney U tests ($\alpha = 0.025$, Bonferroni-corrected) were performed on these metrics to assess statistical differences among the dosiomics-driven and clinical TCP models.

3. Results

3.1. Time-to-event analysis

The LETd maps led to the best performing time-to-event model, reaching a test C-index of 0.750 and 0.786 with r-Cox and s-SVM, respectively. D_{RBE} and D_{PHYS} showed comparable results for r-Cox

models with a test C-index assessed at 0.750, while their performance degraded to 0.536 and 0.643 respectively, in case of s-SVM. The median cross-validation C-index described instead a more uniform scenario on both r-Cox and s-SVM, as all three maps exhibited a comparable performance, with no statistical differences (Fig. 2, $p > 0.05$). In this regard, both models built on clinical parameters showed promising performances on CV, despite a poor generalization capability on the test set, with C-indexes decreasing from 0.80 and 0.82 in CV for s.SVM and r-Cox, to 0.536 in the test. The C-index from CV and test are summarized in Table 2.

The estimated Kaplan Meier curves (Fig. 3 and Fig. S1, S2) significantly separated low-risk from high-risk patients ($p < 0.0125$) in all the examined scenarios, with the D_{PHYS}-based models ($p = 0.047$) and the s-SVM trained with D_{RBE} features ($p = 0.083$) showing a non-significative separation. In particular, LET_d based models showed the most effective stratification ($p = 0.0121$, for both r-Cox and s-SVR models) together with D_{RBE}, which nonetheless was characterized by a poorer performance in terms of C-index. On the other hand, the KM estimated through clinical parameters could not separate the two classes significantly, with a p-value of the log-rank test highly above the acceptability threshold.

Supplementary materials S2 collects the features selected for each map: *Shape_Elongation* is the only feature to be selected in all cases, being always significantly separated between LC/LR classes and high/low risk stratifications by the best performing models on the test set. Each map was characterized by a different feature set composed of both first order and texture features, with D_{RBE} having a significantly lower *mean* and *10th percentile* in LR and high risk patients against LC and low risk (Fig. S3). Similarly, *mean absolute deviation* of D_{PHYS} was significantly lower in LC and low risk cases. D_{PHYS} *Cluster Prominence* is the only texture feature to be significantly separated both ahead (LC/LR) and downstream of stratification (High/Low Risk, Fig. S4). A lower value of LET_d *Glszm SmallAreaLowGrayLevelEmphasis* and *Glszm LowGrayLevelZoneEmphasis* (Fig. S5) in LC and Low Risk patients can be noted, although these differences do not maintain statistical significance both ahead and downstream of stratification.

3.2. TCP models

The selected feature sets were used to define the dosiomics-driven TCPs and compare them with a clinical data-driven TCP that was considered as reference. The median coefficients of the logistic function used to define the dosiomics score are summarized in Table S1 in supplementary material S3. Table 3 collects the f-score and accuracy values for the TCP models in both CV and test (visualized in Fig. S6 in supplementary material). The LETd based TCP (Fig. 4) reached the best performance among the others with an f-score of 0.75 and an accuracy of 0.82 on the test set. The clinical TCP model (Fig .4) showed a poor performance with an f-score of 0.25 and an accuracy of 0.45, similarly to the D_{RBE} and D_{PHYS} models (Shown in Fig. S7 in supplementary material) with 0.40 and 0.45 respectively. Considering the performance on CV, the TCP model built on LETd features reached a significatively higher f-score with respect to the clinical one ($p < 0.025$), while D_{PHYS} achieved a significatively higher accuracy.

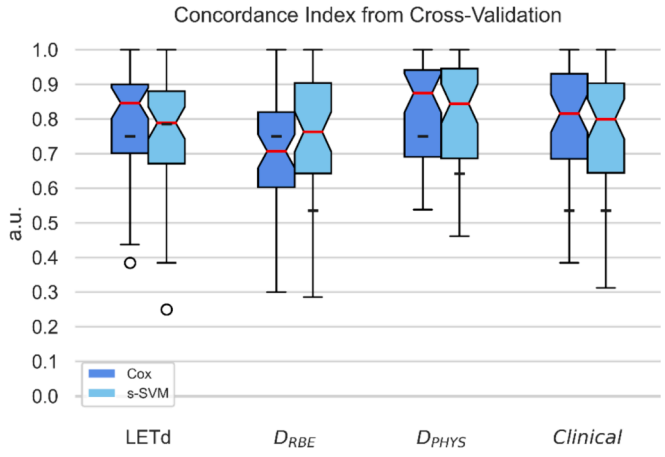

Fig. 2. C-index for r-Cox and s-SVM models. The box includes the IQR and the median value (Red) relative to the cross-validation, whiskers delimits the points within 1.5 * IQR. The results on the test set are displayed with the black solid horizontal segment line.

Table 2
Harrell's C-index for r-Cox and s-SVM models [*median/IQR*]. * denotes significant KM curves ($p < 0.0167$).

	r-Cox			
	LET_d	**D_{RBE}**	**D_{PHYS}**	**Clinical**
CV	0.846/0.239	0.707/0.237	0.875/0.262	0.816/0.244
test	0.750*	0.750*	0.750	0.536
	s-SVM			
	LET_d	**D_{RBE}**	**D_{PHYS}**	**Clinical**
CV	0.788/0.224	0.763/0.264	0.844/0.254	0.80/0.322
test	0.786*	0.536	0.643	0.536

4. Discussion

The present study proposed a dosiomics approach to physical, RBE-weighted dose and LET_d maps, with the aim of investigating two different time-to-event models, namely r-Cox and s-SVM, and effectively stratify patients on the base of the risk of developing LR. Along with this, a dosiomics-based TCP was defined from each optimal features set and compared with a clinical TCP model including relevant prognostic factors as suggested in the literature [2].

All dosiomics time-to-event models showed a median CV C-index above 0.70. The performance of the LET_d models was very promising, with a C-index of 0.75 and 0.789 in the test set, for r-Cox and s-SVM respectively. These results allowed achieving a significant separation between low- and high-risk patients ($p = 0.0121$), as shown by the KM curves in Fig. 3. Differently, the optimal performances of D_{PHYS} and clinical parameters in CV (C-index > 0.8) were not reflected on the test set, with a non-significant patients' stratification. D_{RBE} Cox model showed a reasonable but lower performance on the time-to-event analysis, despite a potential prognostic power of D_{RBE} features in effectively separate patients in low/high risk of LR ($p = 0.012$).

The relevance of tumor shape (i.e. *Shape_Elongation*) in predicting LR has been confirmed, as previously indicated by Buizza et al. and earlier studies that correlated tumor size and shape with treatment outcomes in SBC [13,14,31,32]. First order statistics described significantly different distributions among patients, while no texture feature proved to be relevant, except for D_{PHYS} *Cluster Prominence* which suggested a higher heterogeneity of physical dose in LR patients. Despite no specific LET_d texture feature proved to be significant both ahead and downstream of stratification, a lower value of *Glszm SmallAreaLowGrayLevelEmphasis* may suggest a more homogeneous distribution of LET_d in the target for LC and low risk patients, and while a higher *Glszm LowGrayLevelZoneEmphasis* (Fig. S3) may suggest the presence of areas of lower LETd in the target for LR and high risk patients.

The feature sets employed for time-to-event analysis were then used to define dosiomics-based TCP models. TCP modelling have been largely investigated in the literature, with multiple data-driven approaches that tried to define a TCP score in relation to radiomics features in the form of nomograms [27], but none with respect to dosiomics signatures including LETd. The proposed analysis showed the LETd and D_{PHYS} TCP models to provide significant improvements with respect to the clinical TCP model in terms of f1-score and accuracy, respectively. This supports the role of dosiomics features within data-driven predictive modeling, towards a personalized evaluation of treatment outcome. Considering

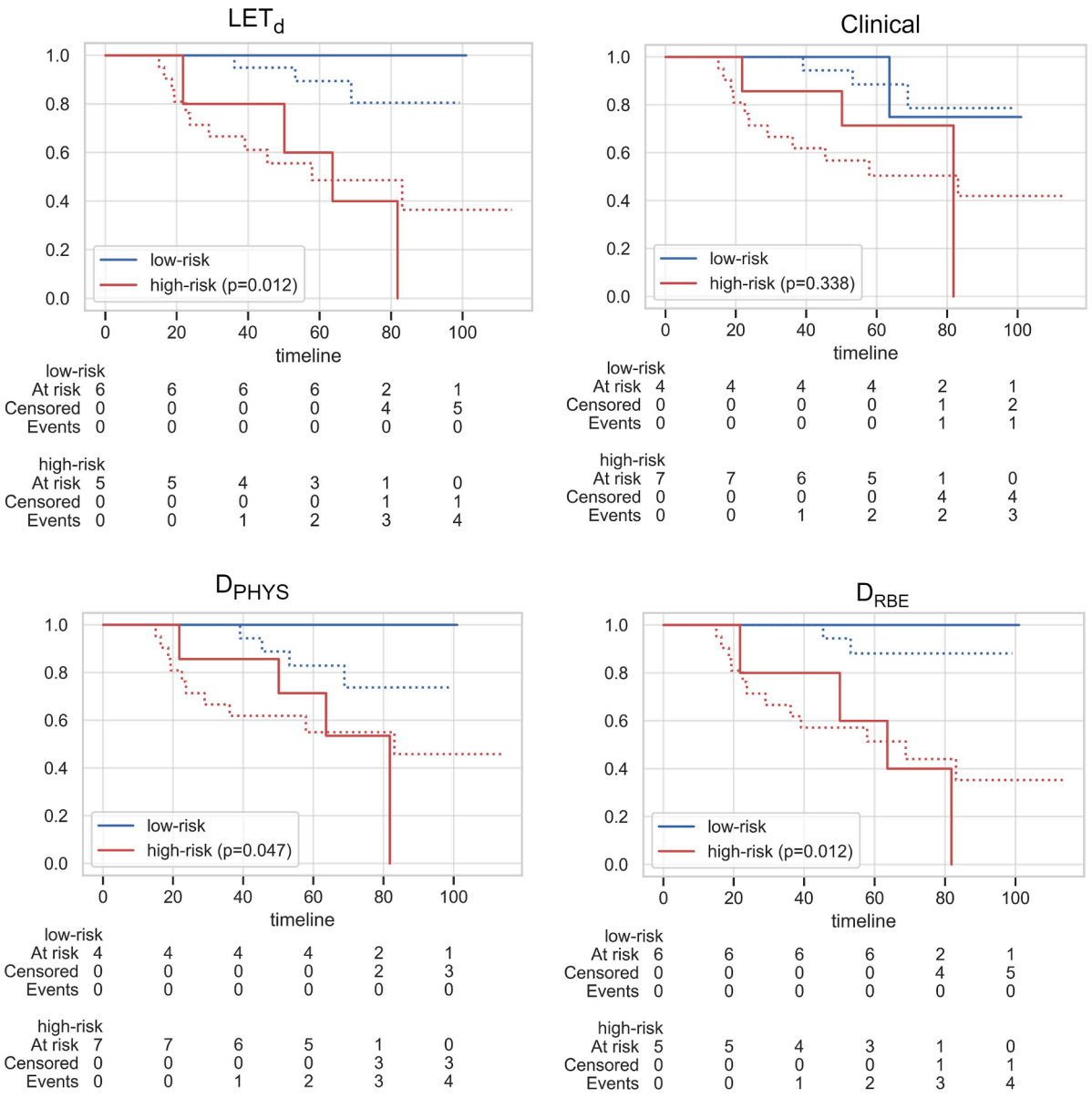

Fig. 3. Estimated Kaplan Maier curves for LET_d, D_{PHYS} and D_{RBE} and clinical parameters. Kaplan–Meier survival curves for patients at high-(red) and low-risk (blue) of LR as stratified by the corrispondent best performing model on the test set (s-SVM for LETd, r-Cox for dose maps and clinical parameters). Solid lines represent the KM curves estimated for the test-set, while dotted lines refer to the training set. Below the plot, the number of test-set patients belonging to each risk group along time (months).

Table 3
f-Score and accuracy relative to the TCP models both on CV and test (median [IQR]). * to indicate a statistically significant difference with respect to the clinical TCP model ($p < 0.025$).

	LET_d		D_{RBE}		D_{PHYS}		Clinical	
	f-score	**acc**	**f-score**	**acc**	**f-score**	**acc**	**f-score**	**acc**
CV	0.67* [0.52–0.70]	0.71 [0.55–0.79]	0.6 [0.48–0.67]	0.71 [0.64–0.76]	0.57 [0.52–0.67]	0.73* [0.65–0.79]	0.40 [0.22–0.52]	0.60 [0.52–0.64]
Test	0.75	0.82	0.4	0.45	0.57	0.73	0.25	0.45

the dosiomics score (Table S1), the coefficients assigned to texture features were relatively high in both D_{RBE} and D_{PHYS}, while the mean absolute deviation was associated with a higher weight if compared to the texture features for LETd. *Shape_Elongation* had a relevant impact in all the dosiomics-based TCP models, proving its role in relation to treatment outcome prediction. Differently, D95 guided the classification on the clinical TCP score, with marginal contributions of GTV volume, sex and OARs involvement.

Despite the relevant findings emerged from the analyses, further evaluations are required. Our results, indeed, must be seen in light of the limited dataset at our disposal, mainly compromised due to the extremely low incidence of SBC and the peculiar treatment employed (i.e., CIRT), as well as the need for long follow-up time (around 5 years, [2,4]) due to the slow-growing nature of SBC. Therefore, the possibility

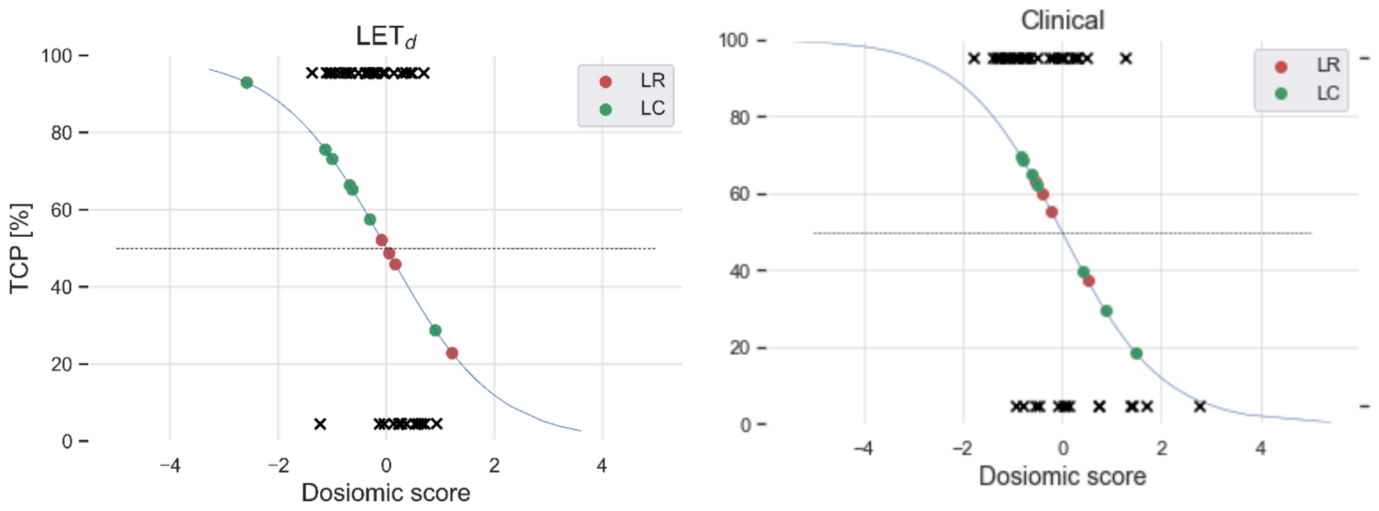

Fig. 4. LETd-based and clinical TCP models. The training set is displayed with the symbol '**X**', while the test data are shown with green (LC) and red (LR) dots. The black dashed line represents the 50% TCP threshold used to discern among low and high risk.

of extending the study to a larger and independent cohort would allow drawing more robust and generalizable conclusions, along with evaluating feature robustness and reproducibility and investigating different feature selection routines to identify stable and relevant features for TCP modeling. In this regard, hybrid models including the best performing features from LETd, dose and clinical parameters could be investigated in future developments and, together with a larger dataset, could represent a significative step towards a personalized treatment modelling in SBC. Furthermore, the exploration of more complex and non-linear modeling techniques, such as SVM classifiers or deep learning approaches, can be considered to better capture the elaborate relationships among data. Despite these limitations, this study poses the basis to further investigate strategies for personalization and optimization of CIRT treatments for skull base chordomas.

5. Conclusion

This work investigated a dosiomics pipeline based on LET_d, physical and RBE-weighted dose maps to evaluate their role in treatment outcome prediction, and allowed defining, for the first time, a dosiomics-based TCP model to predict LR in SBC after CIRT. Our analysis suggests that both LET_d and dose maps could be relevant sources of prognostic factors for LR in skull base chordomas treated with CIRT. In particular, LET_d showed more consistent results in terms of C-index and significance of KM curves, along with a TCP model stratifying patients with promising sensitivity and precision if compared to the clinical one.

Declaration of competing interest

The authors declare that they have no known competing financial interests or personal relationships that could have appeared to influence the work reported in this paper.

Acknowledgements

This work was supported by AIRC (Associazione Italiana per la Ricerca sul Cancro) IG2020 - 24946.

Appendix A. Supplementary data

Supplementary data to this article can be found online at https://doi.org/10.1016/j.ejmp.2024.103421.

References

[1] Yaniv D, Soudry E, Strenov Y, Cohen MA, Mizrachi A. Skull base chordomas review of current treatment paradigms. World J Otorhinolaryngol Head Neck Surg 2020;6:125–31. https://doi.org/10.1016/j.wjorl.2020.01.008.
[2] Iannalfi A, D'Ippolito E, Riva G, Molinelli S, Gandini S, Viselner G, et al. Proton and carbon ion radiotherapy in skull base chordomas: a prospective study based on a dual particle and a patient-customized treatment strategy. Neuro Oncol 2020;22:1348–58. https://doi.org/10.1093/neuonc/noaa067.
[3] Holtzman AL, Seidensaal K, Iannalfi A, Kim KH, Koto M, Yang W-C, et al. Carbon ion radiotherapy: an evidence-based review and summary recommendations of clinical outcomes for skull-base chordomas and chondrosarcomas. Cancers (Basel) 2023;15:5021. https://doi.org/10.3390/cancers15205021.
[4] Frezza AM, Botta L, Trama A, Dei Tos AP, Stacchiotti S. Chordoma: update on disease, epidemiology, biology and medical therapies. Curr Opin Oncol 2019;31:114–20. https://doi.org/10.1097/CCO.0000000000000502.
[5] Samii A, Gerganov VM, Herold C, Hayashi N, Naka T, Mirzayan MJ, et al. Chordomas of the skull base: surgical management and outcome. J Neurosurg 2007;107:319–24. https://doi.org/10.3171/JNS-07/08/0319.
[6] Stacchiotti S, Gronchi A, Fossati P, Akiyama T, Alapetite C, Baumann M, et al. Best practices for the management of local-regional recurrent chordoma: a position paper by the chordoma global consensus group. Ann Oncol 2017;28:1230–42. https://doi.org/10.1093/annonc/mdx054.
[7] O'Connor JPB, Aboagye EO, Adams JE, Aerts HJWL, Barrington SF, Beer AJ, et al. Imaging biomarker roadmap for cancer studies. Nat Rev Clin Oncol 2017;14:169–86. https://doi.org/10.1038/nrclinonc.2016.162.
[8] Lambin P, Leijenaar RTH, Deist TM, Peerlings J, de Jong EEC, van Timmeren J, et al. Radiomics: the bridge between medical imaging and personalized medicine. Nat Rev Clin Oncol 2017;14:749–62. https://doi.org/10.1038/nrclinonc.2017.141.
[9] Liang B, Yan H, Tian Y, Chen X, Yan L, Zhang T, et al. Dosiomics: extracting 3D spatial features from dose distribution to predict incidence of radiation pneumonitis. Front Oncol 2019;9. https://doi.org/10.3389/fonc.2019.00269.
[10] Wei W, Wang K, Liu Z, Tian K, Wang L, Du J, et al. Radiomic signature: a novel magnetic resonance imaging-based prognostic biomarker in patients with skull base chordoma. Radiother Oncol 2019;141:239–46. https://doi.org/10.1016/j.radonc.2019.10.002.
[11] Yamazawa E, Takahashi S, Shin M, Tanaka S, Takahashi W, Nakamoto T, et al. MRI-based radiomics differentiates skull base chordoma and chondrosarcoma: a preliminary study. Cancers (Basel) 2022;14:3264. https://doi.org/10.3390/cancers14133264.
[12] Li L, Wang K, Ma X, Liu Z, Wang S, Du J, et al. Radiomic analysis of multiparametric magnetic resonance imaging for differentiating skull base chordoma and chondrosarcoma. Eur J Radiol 2019;118:81–7. https://doi.org/10.1016/j.ejrad.2019.07.006.
[13] Buizza G, Paganelli C, D'Ippolito E, Fontana G, Molinelli S, Preda L, et al. Radiomics and dosiomics for predicting local control after carbon-ion radiotherapy in skull-base chordoma. Cancers (Basel) 2021;13:339. https://doi.org/10.3390/cancers13020339.
[14] Morelli L, Parrella G, Molinelli S, Magro G, Annunziata S, Mairani A, et al. A dosiomics analysis based on linear energy transfer and biological dose maps to predict local recurrence in sacral chordomas after carbon-ion radiotherapy. Cancers (Basel) 2022;15:33. https://doi.org/10.3390/cancers15010033.
[15] Molinelli S, Magro G, Mairani A, Allajbej A, Mirandola A, Chalaszczyk A, et al. How LEM-based RBE and dose-averaged LET affected clinical outcomes of sacral chordoma patients treated with carbon ion radiotherapy. Radiother Oncol 2021;163:209–14. https://doi.org/10.1016/j.radonc.2021.08.024.

[16] Matsumoto S, Lee SH, Imai R, Inaniwa T, Matsufuji N, Fukahori M, et al. Unresectable chondrosarcomas treated with carbon ion radiotherapy: relationship between dose-averaged linear energy transfer and local recurrence. Anticancer Res 2020;40:6429–35. https://doi.org/10.21873/anticanres.14664.
[17] Liu C, Patel SH, Shan J, Schild SE, Vargas CE, Wong WW, et al. Robust optimization for intensity modulated proton therapy to redistribute high linear energy transfer from nearby critical organs to tumors in head and neck cancer. Int J Radiat Oncol* Biolo* Phys 2020;107:181–93. https://doi.org/10.1016/j.ijrobp.2020.01.013.
[18] Inaniwa T, Kanematsu N, Noda K, Kamada T. Treatment planning of intensity modulated composite particle therapy with dose and linear energy transfer optimization. Phys Med Biol 2017;62:5180–97. https://doi.org/10.1088/1361-6560/aa68d7.
[19] Cao W, Khabazian A, Yepes PP, Lim G, Poenisch F, Grosshans DR, et al. Linear energy transfer incorporated intensity modulated proton therapy optimization. Phys Med Biol 2017;63:015013. https://doi.org/10.1088/1361-6560/aa9a2e.
[20] Hahn C, Heuchel L, Ödén J, Traneus E, Wulff J, Plaude S, et al. Comparing biological effectiveness guided plan optimization strategies for cranial proton therapy: potential and challenges. Radiat Oncol 2022;17:169. https://doi.org/10.1186/s13014-022-02143-x.
[21] Giantsoudi D, Grassberger C, Craft D, Niemierko A, Trofimov A, Paganetti H. Linear energy transfer-guided optimization in intensity modulated proton therapy: feasibility study and clinical potential. Int J Radiat Oncol* Biol* Phys 2013;87:216–22. https://doi.org/10.1016/j.ijrobp.2013.05.013.
[22] Coates JTT, Pirovano G, El Naqa I. Radiomic and radiogenomic modeling for radiotherapy: strategies, pitfalls, and challenges. J Med Imaging 2021;8. https://doi.org/10.1117/1.JMI.8.3.031902.
[23] El Naqa I, Bradley J, Blanco AI, Lindsay PE, Vicic M, Hope A, et al. Multivariable modeling of radiotherapy outcomes, including dose-volume and clinical factors. Int J Radiat Oncol* Biol* Phys 2006;64:1275–86. https://doi.org/10.1016/j.ijrobp.2005.11.022.
[24] Strigari L, Benassi M, Sarnelli A, Polico R, D'Andrea M. A modified hypoxia-based TCP model to investigate the clinical outcome of stereotactic hypofractionated regimes for early stage non-small-cell lung cancer (NSCLC). Med Phys 2012;39:4502–14. https://doi.org/10.1118/1.4730292.
[25] Webb S, Nahum AE. A model for calculating tumour control probability in radiotherapy including the effects of inhomogeneous distributions of dose and clonogenic cell density. Phys Med Biol 1993;38:653–66. https://doi.org/10.1088/0031-9155/38/6/001.
[26] Buizza G, Molinelli S, D'Ippolito E, Fontana G, Pella A, Valvo F, et al. MRI-based tumour control probability in skull-base chordomas treated with carbon-ion therapy. Radiother Oncol 2019;137:32–7. https://doi.org/10.1016/j.radonc.2019.04.018.
[27] Luo L-M, Huang B-T, Chen C-Z, Wang Y, Su C-H, Peng G-B, et al. A combined model to improve the prediction of local control for lung cancer patients undergoing stereotactic body radiotherapy based on radiomic signature plus clinical and dosimetric parameters. Front Oncol 2022;11. https://doi.org/10.3389/fonc.2021.819047.
[28] Zwanenburg A, Leger S, Vallières M, Löck S. Image Biomarker Standardisation Initiative 2016. https://doi.org/10.1148/radiol.2020191145.
[29] Harrell FE, Lee KL, Mark DB. Multivariable prognostic models: issues in developing models, evaluating assumptions and adequacy, and measuring and reducing errors. Stat Med 1996;15:361–87. https://doi.org/10.1002/(SICI)1097-0258(19960229)15:4<361::AID-SIM168>3.0.CO;2-4.
[30] McKnight PE, Najab J. Mann-Whitney <scp>U</Scp> Test. In The Corsini Encyclopedia of Psychology: Wiley; 2010. p. 1.
[31] Limkin EJ, Reuzé S, Carré A, Sun R, Schernberg A, Alexis A, et al. The complexity of tumor shape, spiculatedness, correlates with tumor radiomic shape features. Sci Rep 2019;9:4329. https://doi.org/10.1038/s41598-019-40437-5.
[32] Teng C, Yang Q, Xiong Z, Ye N, Li X. Multivariate analysis and validation of the prognostic factors for skull base chordoma. Front Surg 2021;8. https://doi.org/10.3389/fsurg.2021.764329.